Contents lists available at ScienceDirect

Carbohydrate Polymers

journal homepage: http://ees.elsevier.com

Injectable bone substitute based on chitosan with polyethylene glycol polymeric solution and biphasic calcium phosphate microspheres

Daniel Bezerra Lima [a,1], Mônica Adriana Araújo de Souza [b,1], Gabriel Goetten de Lima [c,d], Erick Platiní Ferreira Souto [b], Hugo Miguel Lisboa Oliveira [e], Marcus Vinícius Lia Fook [a], Marcelo Jorge Cavalcanti de Sá [b,d,*]

[a] Unidade Académica de Engenharia dos Materiais - CERTBIO, Universidade Federal de Campina Grande, Campina Grande, Paraíba, Brazil
[b] Programa de Pós-Graduação em Medicina Veterinária - PPGMV, Universidade Federal de Campina Grande, Campina Grande, Paraíba, Brazil
[c] Programa de Pós-Graduação em Engenharia e Ciência dos Materiais - PIPE, Universidade Federal do Paraná, Curitiba, Paraná, Brazil
[d] Materials Research Institute, Athlone Institute of Technology, Athlone, Ireland
[e] Unidade Académica de Engenharia dos Alimentos, Universidade Federal de Campina Grande, Campina Grande, Paraíba, Brazil

ARTICLE INFO

Keywords
Injectable bone substitute
Biphasic calcium phosphate
Microspheres
Tibial bone defect

ABSTRACT

We described a method to produce an injectable bone substitute consisting of a solid and liquid phase, this solid was formed using the coacervation method consisting of a mixture of Hydroxyapatite (HAp) and beta-Tricalcium Phosphate (β-TCP) which the sodium alginate - precursor - was removed during sinterization. The biphasic calcium phosphate microspheres had varying size distributions depending on the flow rate and these microspheres were mixed with a polymeric solution, chitosan and polyethylene glycol, and depending on the ratio of these phases, the injectability results varied. Nonetheless, the force required for complete removal will not disrupt the accuracy of injection into the bone defect while the biomaterial exhibited no cytotoxicity with promising results from *in vivo* using tibia bone defect in rabbits at 30 and 60 days whereas bone repair was more intense and accentuated with the usage of the biomaterial, and was gradually absorbed during the evaluated periods.

1. Introduction

Alternative strategies have been developed for a faster regeneration without the drawbacks that usually occurs within long term implants (Cordova et al., 2014), while also owning osteostimulation and biodegradation; therefore, bioceramics are considered as an agreeable candidate (Canillas, Pena, de Aza, & Rodríguez, 2017; Kokubo, 2008). Certain bioceramics containing calcium phosphate have its structure and chemistry similar to the minerals of the native bone, besides having good biocompatibility and osteoconductivity (Kraal et al., 2008); such as hydroxyapatite (HAp) and beta-tricalcium phosphate (β-TCP) (Rangavittal, Landa-Canovas, Gonzalez-Calbet, & Vallet-Regí, 2000).

However, hydroxyapatite is brittle when in porous form with weak bioactivity to induce osteogenesis and angiogenesis (Nam, Bae, Moon, & Kang, 2006); also, β-TCP is more unstable and more susceptible to degradation than hydroxyapatite (Wang, Pan et al., 2019). Nonetheless, the mixture of this two compounds labelled as biphasic calcium phosphate (BCP) is widely used in bone tissue engineering due to unique characteristics (Lee, Makkar, Paul, & Lee, 2017; Legeros, Lin, Rohanizadeh, Mijares, & Legeros, 2003). Implants containing biphasic calcium phosphate have been shown to increase bone regeneration due to its porosity being similar to the osteon cells, allowing cells to attach, migrate and proliferate easier in the affected site (Abueva, Jang, Padalhin, & Lee, 2017).

Current research has been focused on reducing the invasiveness when materials are implanted into the wound site, such as the usage of microsphere granules that can be added into irregular bone defects (Thangavelu et al., 2019). However, regardless of the ceramic used as implant material, they are considered to be difficult to work with due to their low weight and repulsive nature which hinders their performance in clinical applications (Taz et al., 2019). Furthermore, porosity from closely packed dried calcium phosphate microspheres is very low (Lal & Sun, 2004). Therefore, a solution to this is to mix with a material that can hold the spheres together by cohesive force while also able to help the bone formation at the defect site.

Within these strategies, stands out the usage of polymeric solutions to produce a slurry that suspends these microspheres calcium phos-

* Corresponding author at: Programa de Pós-Graduação em Medicina Veterinária - PPGMV, Universidade Federal de Campina Grande, Campina Grande, Paraíba, 58708-110, Brazil.
E-mail address: mjcdesa@gmail.com (M.J.C. de Sá)
[1] These authors contributed equally to this manuscript.

https://doi.org/10.1016/j.carbpol.2020.116575
Received 16 January 2020; Received in revised form 6 April 2020; Accepted 2 June 2020
Available online xxx
0144-8617/

phates for an easily injectable material - injectable bone substitute (IBS) (Daculsi, 1998). IBS has been used to minimally invasive surgery while also owning excellent physicochemical properties, they can also stuff complex-shaped cavities from bones when injected, lowering the risk of infection and ability to repair and regenerate bone tissue successfully (Thai & Lee, 2010).

Particularly, the usage of chitosan for bone regeneration is one of the most studied materials proving to promote bone growth (Di Martino, Sittinger, & Risbud, 2005) through increased osteoblast deposition on mineral rich matrixes. Likewise, chitosan has weak mechanical properties and quick degradation (Li, Zhang, & Zhang, 2018); therefore, studies of chitosan with calcium phosphate shows an enhance to the mechanical strength of the inorganic phase, reduces the degradation rate and enhance the regeneration when used as a scaffold for bone regeneration applications (Saravanan, Vimalraj, Thanikaivelan, Banudevi, & Manivasagam, 2019).

Despite the fact that it is possible to obtain IBS with in-situ hardening (Jahan, Mekhail, & Tabrizian, 2019; Moreira, Carvalho, Mansur, & Pereira, 2016); they are still considered to be insufficient for providing support for bone regeneration (Hasan et al., 2019). Nonetheless, the usage of soft scaffolds for endochondral ossification – occurring during healing of fractured long bones – can help mimic the microenvironment of osteogenic cells and exhibit promotion of bone regeneration compared to monolithic materials (Pon-On et al., 2016).

An injectable scaffold composed of an inorganic and organic phase presents advantages when compared to bone grafts or pre-formed scaffolds such as the ability of the injectable scaffold to flow and fill the bone cavity or defect. In opposition, while using the other type of scaffolds, the surgeon has to shape the material or carve the tissue so the graft can fit the surgical site. These procedures typically require more surgery time and can causa additional trauma with increased risk of infection (Bencherif et al., 2012). Our group recently investigated the injectability properties of a polymeric solution containing chitosan with polyethylene glycol, which exhibits unique features that can act as a carrier for bioceramics (Lima et al., 2018). However, the bone regeneration capability of this injectable material containing a liquid phase of chitosan with polyethylene glycol must be investigated when a bioceramic, solid phase, is presented. Consequently, this work studies the biological and characteristic properties of an IBS consisting of a solid and liquid phase for bone regeneration in rabbit tibial defect model.

2. Materials and methods

2.1. Fabrication of the injectable bone substitute (IBS)

The injectable bone substitute in this work is composed of a mixture of two phases was used – a mixture of liquid and a solid phase.

2.1.1. Production of β-TCP

To obtain β-TCP ($Ca_3(PO_4)_2$) it follows the procedure from (Barbosa et al., 2020) with slightly modifications; 100 g of tribasic calcium phosphate ($Ca_5(PO_4)_3OH$) (Synth) was added in 200 ml of distilled water and homogenized in a mechanical stirrer. After homogenization, 5.3 ml of 85 % phosphoric acid (H_3PO_4) (Synth) was added, slowly under mechanical stirring for 20 min. Subsequently, the mixture was poured into a glass refractory and oven dried at 80 °C for 24 h. After 24 h, the ceramic material was ground with the aid of a sifted mortar, placed in an alumina capsule and baked at 1000 °C for 2 hs.

2.1.2. Solid phase production (BCP - Biphasic Calcium Phosphate microspheres)

For the solid phase of the IBS, the biphasic CaPs granules were formed from a mixture of 25 % HAp and 75 % β-TCP. An aqueous slurry was prepared using mechanical stirring, with paddle blades, at 500 rpm for 24 h. The aqueous slurry was composed of 343.125 g final solution containing 300 ml of distilled water, 5.25 g of sodium alginate (Vetec, Brazil), 9.375 g of HAp (Sigma-Aldritch, Brazil), 28.125 g of β-TCP and 0.375 μl of a dispersant based on ammonium methacrylate (LIOSPERSE® 511, Miracema- Nuodex, Brazil). The paste was introduced into a syringe with 18.8 mm internal diameter connected to a hose of 3 mm diameter and 20 cm long, having at the end a two-fluid atomizing nozzle. The flow rate of the paste was adjusted in three variations (50 mL/h, 70 mL/h and 90 mL/h). The aqueous slurry was atomized by a 0.6 mm diameter nozzle with a fixed pressure of 0.4 bar above a vessel containing 0.1 M of calcium chloride solution to coagulate the alginate present in the droplets. Afterwards, the spheres were filtered and dried at room temperature, 25.0 ± 2 °C, for 24 h (Fig. 1.1-6 and A).

After drying all spheres, they were sintered in the same batch for a period of 2 h at 900 °C with a heating rate of 5 °C/min in order to degrade and remove the sodium alginate and the dispersant while also able to form a stable, porous structure consisting of calcium phosphate. The temperature of 900 °C was optimized from prior tests as it can completely remove the sodium alginate during sinterization and it is also the beginning of the densification process, that starts from 900 °C and goes below 1125 °C, whereas higher temperature leads to phase transformation of β-TCP to α-TCP.

2.1.3. Liquid phase production (chitosan + PEG400)

The liquid phase in the form of a hydrogel composed of chitosan (CHI) and polyethylene glycol (PEG400) was produced following the methodology of our previous work (Lima et al., 2018). Briefly, chitosan (Medium Molecular Weight, Sigma-Aldrich, degree of deacetylation = 85 %, Molecular Weight = 260 kDa) was dissolved in acetic acid 1.5 % wt following addition of PEG400 (Sigma-Aldrich) 7.5 % wt. by mechanically stirring, using paddle blades at 500 rpm at 25.0 ± 2 °C until complete solubilization (visual disappearance of chitosan particles) (Fig. 1.b) and the final chitosan solution pH was 4.98.

2.1.4. Injectable bone substitute formation (IBS)

Mixing of the phases was carried out by mechanically stirring, while the proportion of the phases for the IBS was investigated at various ratios; which ranged from 0.8 g to 1.0 g / g; i.e., 0.8–1.0 g of liquid phase (continuous phase) was added to 1 g of solid phase. Two sets of solid phases were also used (70 ml/h and 90 ml/h) for the formation of the IBS. Therefore, the nomenclature for the samples is S1C1, consisting of 1 g solid phase +1 g continuous phase or S1C0.8 consisting 1 g solid phase +0.8 g of continuous phase which would be accompanied by the flow rate used. Mixture from the two phases resulted in a putty-like consistency – mouldable and homogeneous. The final IBS sample was added to a syringe to facilitate its application (Fig. 1.c) with its pH at 5.5.

2.2. Injectable bone substitute (IBS) characterisation

2.2.1. X ray diffraction (XRD)

X-ray diffraction analysis were conducted at 25.0 ± 2 °C using a Shimadzu XRD 7000 X-ray diffractometer with copper Kα radiation (1.5418 Å), 40 kV voltage and 30 mA current, examined with a 2θ interval of 10, 0 and 60.0 degrees at a speed of 2θ / min. The diffraction graphs were identified by referring to JCPDS card files and refining of the spectra was performed with the help of X'Pert HighScore Plus software.

2.2.2. Morphology and particle size

The samples were morphologically characterized by Scanning Electron Microscope using two types of equipment, Phenom Pro X (Thermo Fisher Scientific, Massachusetts, USA) model to characterize the BCP microspheres, while FE-SEM S-4700 (HITACHI, Tokyo, Japan) to char-

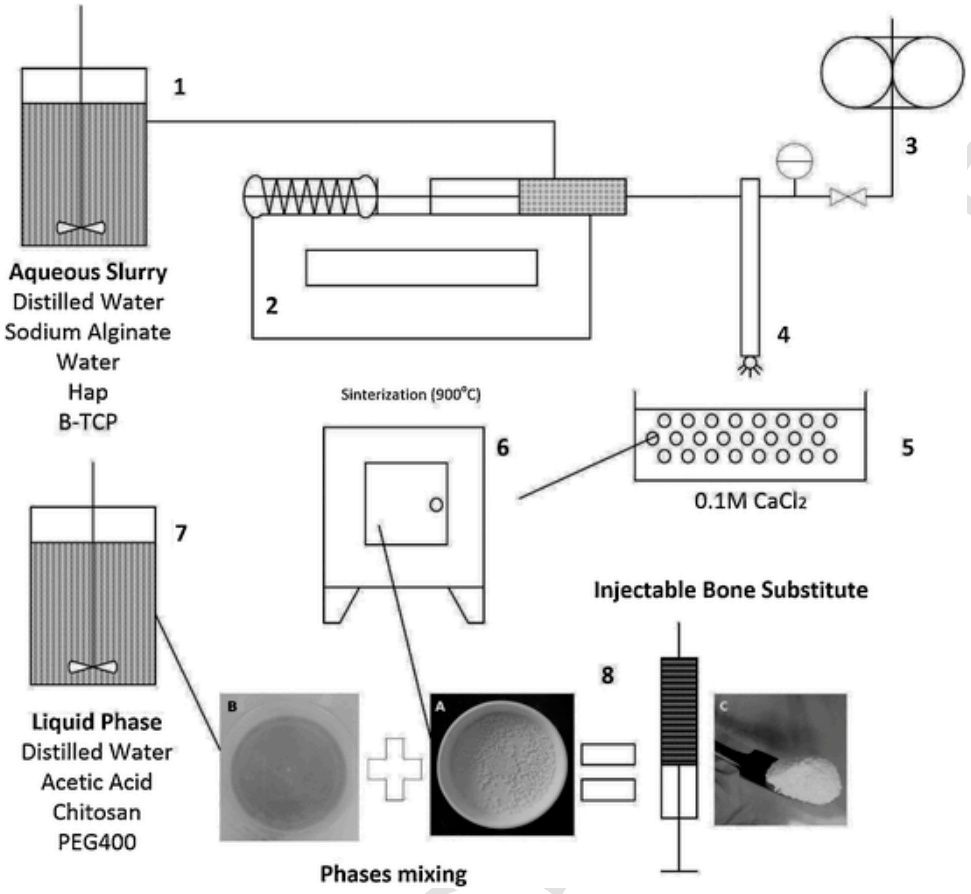

Fig. 1. Injectable bone substitute process apparatus: 1- Aqueous slurry preparation; 2 – Syringe pump; 3 – Air compressor; 4 – Two fluid nozzle; 5- Coacervation Bath; 6 – Sintering Furnace; 7 – Liquid phase preparation; 8 – Final phases mixing into the injectable bone substitute. A) Biphasic ceramic microspheres; B) Chitosan Liquid Phase; C) Final IBS aspect.

acterize the samples of *in vivo* biological tests. For the particle size analysis of the material, direct measurements of the micrographs were made using ImageJ and for each sample, 100 measurements were performed from different micrographs.

2.2.3. Rheological measurements

Viscosity and torque measurements were made on IBS formulations using a Brookfield viscometer (RV + model, Brookfield Engineering Laboratories Inc., MA, USA) at temperature of 25 ± 1 °C with nine spindle speeds (50, 60, 70, 75, 80, 90, 100, 105, 120,135, 140, 150, 160, 180, 200 rpms). Spindle no: seven was used to get all readings within a torque range of 15–80% which resulted in different shear rates depending on the rotation speed. The temperature was maintained using a thermostatically controlled water bath. Torque values were taken and a rest period of 30 s was used between each spindle speed and all experiments were replicated three times. Average shear stress and shear rates were calculated by the method of Mitschka (Mitschka, 1982) and the experimental results were modeled using the Ostwald-de-Waelle (power law) Eq. 1.

$$\mu_{app} = K \bullet \gamma^{n-1} \tag{1}$$

Where, μ_{app} is the apparent viscosity (Pa.s), K is the consistency index (Pa.s^n), γ is the shear rate (s^{-1}) and n is the flow behavior index.

2.2.4. Injectability

The force required to remove IBS from a syringe was determined using an Instron 3366 Universal Mechanical Testing Machine using the methodology developed by (Lima et al., 2018). Briefly, the tests were performed on all sample's conditions using compression mode with a crosshead speed of 20 mm/min and travel set to 20 mm with a 500 N load cell. The time and load required to empty the syringe were recorded. Theoretical calculations were performed using the Eq. 2 developed by (Lima et al., 2018)

$$F = \frac{2^{n+2} \bullet \left(\frac{3 \bullet n+1}{n}\right)^n L \bullet K \bullet \overline{V^n}}{D^{n+1}} \bullet A_{plunger} + F_0 \tag{2}$$

Where, F is the injectability force, D is the syringe tip diameter, L is the length of the syringe, V is the withdrawal speed, A is the area of the syringe plunger and F_0 is the force applied on a blank test.

2.2.5. Mechanical tests

Instrumental texture measurements were preformed using a penetrometer (TA-TX plus, Stable Micro Systems, UK) equipped with a 50 N load cell. An A/BE-d35 probe was compressed twice against each IBS formulation to a defined depth (20 mm) at a rate of 2.0 mm/s. Measurements were performed in triplicate with the probe being extensively washed first with 0.15 M acetic solution followed by distilled water. As a result of these experiments, force-time curves were built and analyzed to determine some mechanical parameters (hardness, adhesiveness, cohesiveness and compressibility) considering the following: Hardness is the force required to attain a given deformation and is given by the altitude of the first peak. Cohesiveness is the ratio between the area under both force-time curve produced in the first and second compression. Compressibility is the work to deform the product during the first penetration and is given by the area under the curve. Adhesiveness is the work necessary to overcome the attractive forces between the surfaces of the sample and the probe and is given by

the area at the negative force region, which means that the probe is no longer penetrating the IBS and is pushing it back.

2.2.6. Cytotoxicity

Several IBS S1C190 samples were sterilized using autoclave at 120 °C for 20 min before the *in vitro* and *in vivo* tests. To evaluate cytotoxicity of IBS, L929 fibroblast cell line (ATCC NCTC clone 929) was used (Rio de Janeiro Cell Bank – BCRJ) grown in RPMI culture medium (RPMI 1640 Medium, Gibco® - Invitrogen Corporation, Grad Island, USA) supplemented with 10 % Fetal Bovine Serum (Gibco®, by Life Technologies) and 1% Antibiotic - Antimycotic (Gibco®, by Life Technologies), kept in 5% CO_2 incubator at 37 °C. The cells used in this experiment followed the standard from *in vitro* cytotoxicity test by BS EN ISO 10993-5: 2009. The cytotoxicity test was performed using a 96-wells plated, each with a cell concentration of 1×10^5 cells/mL in. The IBS tested for cytotoxicity was the S1C190. Cell viability was determined after three days.

2.3. In vivo surgery procedure

The experiments were carried out after approval by the Ethics Committee on the Usage of Animals of UFCG according to approval protocol no. 049/2019.

2.3.1. Characteristics of the animals studied

Twelve adult New Zealand rabbits, nine males and three females, with average of 2.49 ± 0.29 kg weight were randomly divided into two experimental groups of six animals for the surgery and each group subdivided into two other subgroups, according to observation periods of 30 and 60 days.

2.3.2. Anaesthesia and surgery procedure

In the preoperative period, the animals after feeding fasting of six hours water for three hours were anesthetized with the association of xylazine hydrochloride at 2% (5 mg/kg) and ketamine hydrochloride at 5% (30 mg/kg) both intramuscularly. About 30 min before surgery, enrofloxacin was used at a dosage of 10 mg/kg, intramuscularly. After removal of the hairs from both pelvic limbs and lumbosacral region, anaesthesia was performed with lidocaine 2% (0.3 ml/kg) and tramadol (1 mg/kg) in all animals.

Two non-critical 2 mm diameter defects were made in the animals, one in the proximal tibial diaphysis and another in the distal diaphysis of each pelvic limb following the model proposed by (Barbosa et al., 2020). An orthopaedic drill was used, with a 2 mm drill bit, under constant irrigation of sodium chloride solution 0.9 % to avoid thermal injury on the edges of the defect. In the right limb (labelled as IBS) the defects were filled with the biomaterial and in the left limb, the orifices were also filled with the biomaterial but with an addition of covering with the bovine collagen membrane (Lumina-Coat, Criteria, Brazil) between the bone and the biomaterial (labelled as IBS-C) in order to prevent the initial growth of fibrous tissue on the biomaterial so as to act as a control group in relation to the right limb implants. Afterwards, implants were fixed to these areas by suturing the musculature with 'X' suture pattern using a polyglactin 910 3-0; which was also used for reduction of dead space and also the skin suture with standard nylon 3-0 Wolff pattern.

2.4. Postoperative evaluation from in vivo

In the postoperative period, the animals received tramadol hydrochloride (10 mg/kg) for 3 days, intramuscularly, and daily cleaning of the surgical wound with 0.9 % NaCl solution for 10 days.

2.4.1. Radiograph evaluation

Simple radiographs in craniocaudal and middle-lateral projection were performed in the immediate postoperative period, while also at 30 and 60 days in order to analyse the regeneration of the bone. The radiographic evaluation was performed following the model proposed by (Barbosa et al., 2020)Barbosa et al. (2020), in order to measure the bone healing of the lesions that are covered by bone callus.

2.4.2. Euthanasia

The animals were euthanized after 30 days (group 1) or 60 days (group 2) administering 2% xylazine (5 mg/kg) and ketamine at 5% (40 mg/kg) both intramuscularly. After 15 min, 1% propofol (5 mg/kg) was administered, followed by potassium chloride 19.1 % (1 ml/kg) both intravenously.

2.4.3. Processing of in vivo samples

After euthanasia, periods of 30 and 60 days, the tibias were removed and sectioned around 1 cm above and below in relation to the implant. For light microscopy, the specimens were immersed in a 10 % buffered formalin solution for 10 days and were subsequently decalcified in nitric acid solution (5%); later, the pieces were included in paraffin and stained by haematoxylin-eosin.

2.4.4. Histology analysis by scanning electron microscopy (SEM)

Samples intended for SEM were immersed in a 2.5 % glutaraldehyde solution in phosphate buffer at 0.1 M with pH between 7.4 and 7.8 followed by dehydration in a graduated series of alcohol. For surface analysis, half of these samples were fractured in the region where the implant was inserted; while the other half were embedded in transparent epoxy resin, and after a period of 24 h, the samples were cut cross-sectionally and polished for visualization of the cellular components involved in the process of regeneration of the bone tissue.

2.4.5. Statistical analysis

For dependent variables, Wilcoxon test was performed, and for independent variables the Mann-Whitney *U* test The level of significance was 5% and the analyses were performed with the statistical program R Core Team, 2015R Core Team (2015).

3. Results and discussion

3.1. Characterization of the solid phase

3.1.1. Solid phase microstructure

After being submitted to 900 °C sintering process, solid phase samples were characterized by XRD (Fig. 2) in order to identify the profile of the calcium phosphate crystalline phases for the final solid phase product. According to the refinement, all ceramic phases used in the study were obtained and at the proportion of 22.891 % for HAp phase (JCPDS card - 090432), and 77.109 % for β-TCP phase (JCPDS card - 090169) with a refinement confidence factor of Rwp = 10.85 %. The presence of hydroxyapatite is confirmed by the main diffraction angles (2θ) at 31.77°, 32.90° and 33.02° that are related to the miller indices of (2 2 1, d = 2.81 Å),(-2 2 2, d = 2.77 Å) and (-3 6 0, d = 2.71 Å). Moreover, the presence of crystalline β -TCP is also confirmed by the angles of 21.87°, 27.76° and 31.02° that harmonize the Miller indices of (0 2 2, d = 4.06 Å) (0 2 4, d = 3.21 Å) and (0 2 10, d = 2.88 Å). The result is similar to the initial mixture; however, the differences are related to the decomposition of HAp into β -TCP at 900 °C (Batista, Silva, Lisboa, & Costa, 2020). Biphasic calcium phosphate is reported to have an abundance of bone apatite-like crystals, and the lower HAp/β-TCP ratio is, the greater the abundance of bone apatite-like crystals that directly bond with natural bone with rapid bone ingrowth. Thus, biphasic calcium phosphate can be tailored by alter-

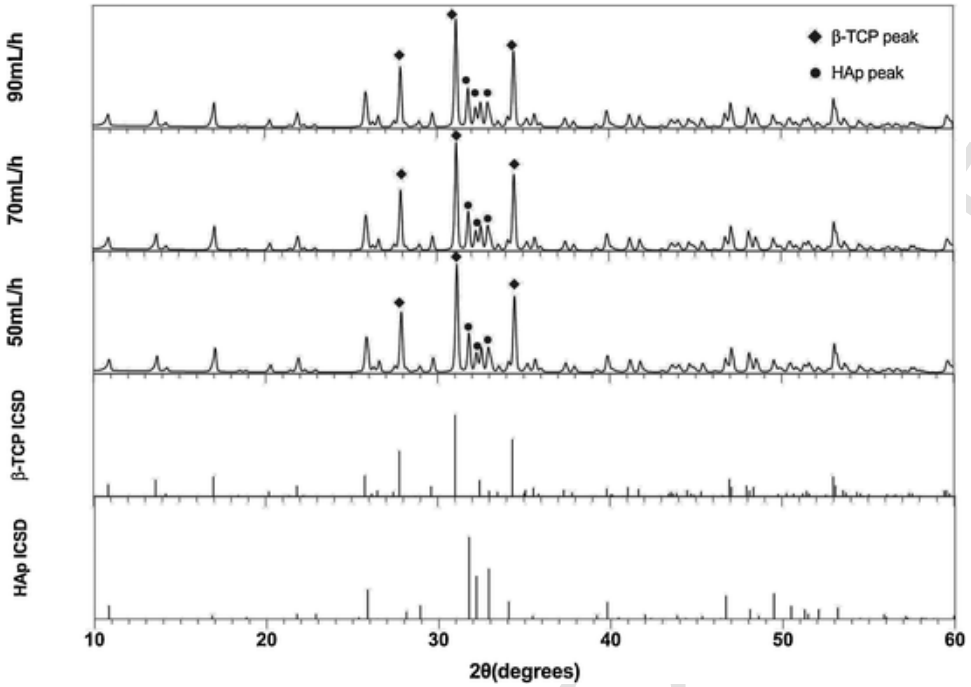

Fig. 2. Diffractograms of the biphasic calcium phosphate microspheres solid phase after refinement. The pure HAp and β-TCP diffractograms are presented for comparison. The main peaks for both phases are highlighted.

ing the ratio of these ceramics to obtain desired characteristics, such as absorption rate and bioactivity, this is due to the preferential dissolution of β-TCP compared to HAp with a slow degradation rate.

3.1.2. Solid phase morphology and size distribution

Fig. 3.A. was generated from the direct observation and measurements of the particle size using SEM micrographs. The mean particle diameter becomes lower for higher feed flow rates in which at 50 ml/

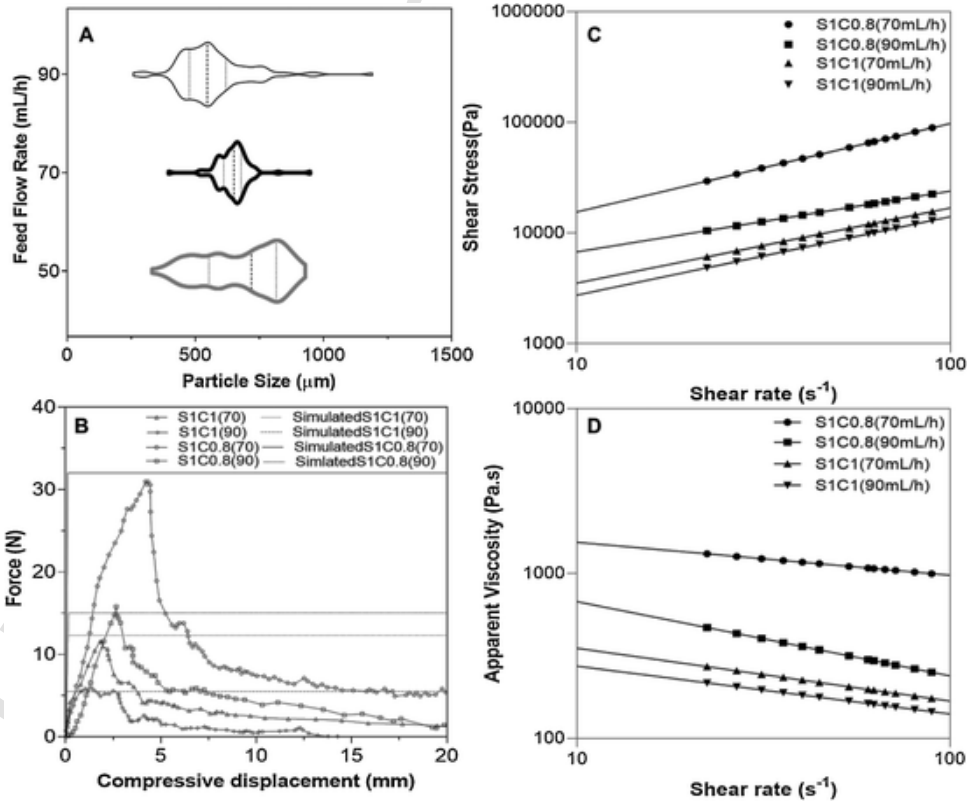

Fig. 3. (A) Violin plot for particle size distribution at three different feed flow rates; (B) Experimental and simulated compression force applied in a 3 ml syringe to the four IBS formulations; and (C) apparent viscosity and flow curves (D) for the four formulations of IBS. All experimental points were fitted with Ostwald-Waele (powder law) model.

h,70 mL/h and 90 mL/h the mean particle size was 680 μm, 646 μm and 567 μm, respectively. Droplet formation with a two-fluid nozzle is a result of a force balance between cohesive forces within the liquid, such as viscosity and surface tension with the gas kinetic energy; therefore, the aqueous slurry could become less viscous and present less cohesive force leading to increased droplets formation and smaller granules. Moreover, feed flow rates of 50 mL/h and 90 mL/h presented higher size dispersibility, with spans of 0.56 while 70 mL/h presented a span of 0.19.

Considering the shape factor, lower feed flow rates provides a more spherical granule in which a flow rate of 50 mL/h and 70 mL/h presented values of 0.86 and 0.84, 90 mL/h presented a value of 0.61 (value of 1 means a perfectly spherical granule). At 90 mL/h more droplets are reaching the coagulation bath, thus the coagulation rate is slower because of calcium availability for alginate bead formation leading to a loosening state on their spherical shape.

Microspheres exhibit a compact aspect expectable after sinterization with a homogenous porous structure, ranging from 1.2 to 3.2 μm for all samples (Fig. 4) with most of the porous caused by the burning and vaporization of alginate at temperatures between 300–500 °C. It is also perceivable the two types of bioceramics used in the study with different morphology and diameters – arrows on Fig. 4.

3.2. Characterization of the IBS composite

3.2.1. Rheological measurements

Four formulations were tested for the IBS by mixing the two phases; the continuous phase(C) (chitosan solution) fraction varied from 1 to 0.8, and the dispersant phase (S) (microspheres) was kept the same while also varying the flow rate. Fig. 3C–D presents the viscosity and the flow curves of the formulations, exhibiting an increase for samples with higher solids fraction following Einstein law of viscosity (Bezerril, de Vasconcelos, Dantas, Pereira, & Fonseca, 2006) and, since 70 mL/h granules have bigger particle size, they occupy a large volume fraction leading to this higher value of viscosity. There is a decrease in viscosity when shear rate is increased on samples, which reflects the non-newtonian behaviour, related to the shear thinning properties (Ramirez Caballero et al., 2019).

A power law equation was fitted to the experimental data to examine the shear thinning behaviour (Table 1), which can reveal the interaction between phases. Interaction between chitosan and the surface of the particles is reported to be *via* hydrogen bonding between hydroxyl group of HAp and the hydroxyl group at position C2 of chitosan, while another possible interaction could be between PO_4^{3-} of both calcium phosphates and the NH_3^+ at position C3 of chitosan (Matinfar, Mesgar, & Mohammadi, 2019). Additionally, chitosan-chitosan interactions can be established by carbonyl and hydroxyl interactions despite the repulsive interaction between the protonated amine. Therefore, as the shear increases, the chitosan chains tend to align in the shear plane and reduces the macromolecular entanglements.

However, granules can constitute entanglement nodes for the chitosan chains *via* the descripted interactions and can be disrupted by the increase of shear rate, leading to different shear thinning behaviours according to the extent of these interactions. Thus, when the solid phase has lower volume fraction (1:1) the shear thinning effect is more pronounced, leading to variation of viscosity at lower and higher shear rates. When the solid phase volume fraction is higher (1:0.8) the IBS approaches the Newtonian behaviour revealing less physical interactions (Jahan et al., 2019). Nonetheless, interaction between β-TCP and chitosan provides a more elastic structure, which is more typical of pseudoplastic fluids than the interaction between HAp and chitosan.

3.2.2. Mechanical properties

Mechanical properties for the IBS samples (Table 1) resulted in no significant differences between samples with the same phase ratio; however, increasing solid content significantly increases hardness and compressibility, so that higher force is required to deform and penetrate the IBS which is due to the ceramic granules that have higher compressive module. Furthermore, the chitosan/peg solution works as lubricant between granules and the chitosan/peg layer may interact with the granule surfaces and could then physically interact with other chitosan chains resulting in a balance between attractive hydroxyl and repulsive protonated amino interactions.

Cohesiveness and adhesiveness are related to the physical interactions such as interchain entanglements and secondary bonds within the material matrix and are related to their stable ability at the application site, they are also dependent of the interaction with the probe and the contact time (Lee, Lim, Israelachvili, & Hwang, 2013). The studied samples resulted in higher values for a smaller phase ratio of continuous, liquid, phase (C) with no variation depending on the flow rate, or granule size. Therefore, chitosan physical interaction with the probe is denser and more probable than the granules-probe.

3.2.3. Injectability

According to ICH Q6A and FDA Guidance for Industry, one of the most important properties of injectable bone substitute is the injectability of the material (Drug, 1998). This property is related to the force required to withdraw the material from the syringe. If too much force is required, the surgeon will have difficulty to apply the material precisely and it was experimentally determined for the four IBS formulations in this work (Table 1 and Fig. 3.B) while it was also estimated the force required to withdraw the IBS. The maximum required force to withdraw the IBS ranges from 5.5 N to 32 N and even though the IBS viscosity is much higher than the viscosity found for the continuous phase (reported previously - (Lima et al., 2018)), the force found for the IBS is rather similar because no metallic syringe tip was used, and thus, the syringe orifice is wider.

The maximum force required to remove the IBS follows a similar trend, whereas the IBS with higher viscosity is also the one that requires more force for withdrawal in accordance with a previous work (Ramirez Caballero et al., 2019). At first, maximum values of force are required for all samples - this is primarily due to the static frictional forces between the IBS and the walls of the syringe and initial resistance - but upon reaching this limit, extrusion forces decrease targeting a constant value for the rest of the injection process.

This maximum compression force depends mainly on the ratio of mixture liquid + solid phases, and subsequently, on the size of microspheres used. There is a further increase in withdrawal force with lower amounts of liquid phase; as it would be expected, since we are reducing the ability of the solid phase to free flow into the liquid. This behaviour follows the pattern of the pure liquid phase injectability results reported before by our group (Lima et al., 2018), meaning that the solid phase does not alter this property. Considering the solid phase from the IBS, the results indicates that decreasing the sphere size led to a further decrease in compressive force. This decrease can also be related to the free flow of the spheres, whereas a higher sphere size leads to a more compact IBS and they can no longer move as easily upon reaching the specific initial glide force from smaller spheres. From all conditions studied in this test, the sample S1C1 using 90 ml/h flow rate for the solid phase had the lowest compressive force profile, with a maximum peak of 5.5 N and stabilizing around 0.5 N until the end of the test, resulting in the IBS of choice for the *in vivo* tests.

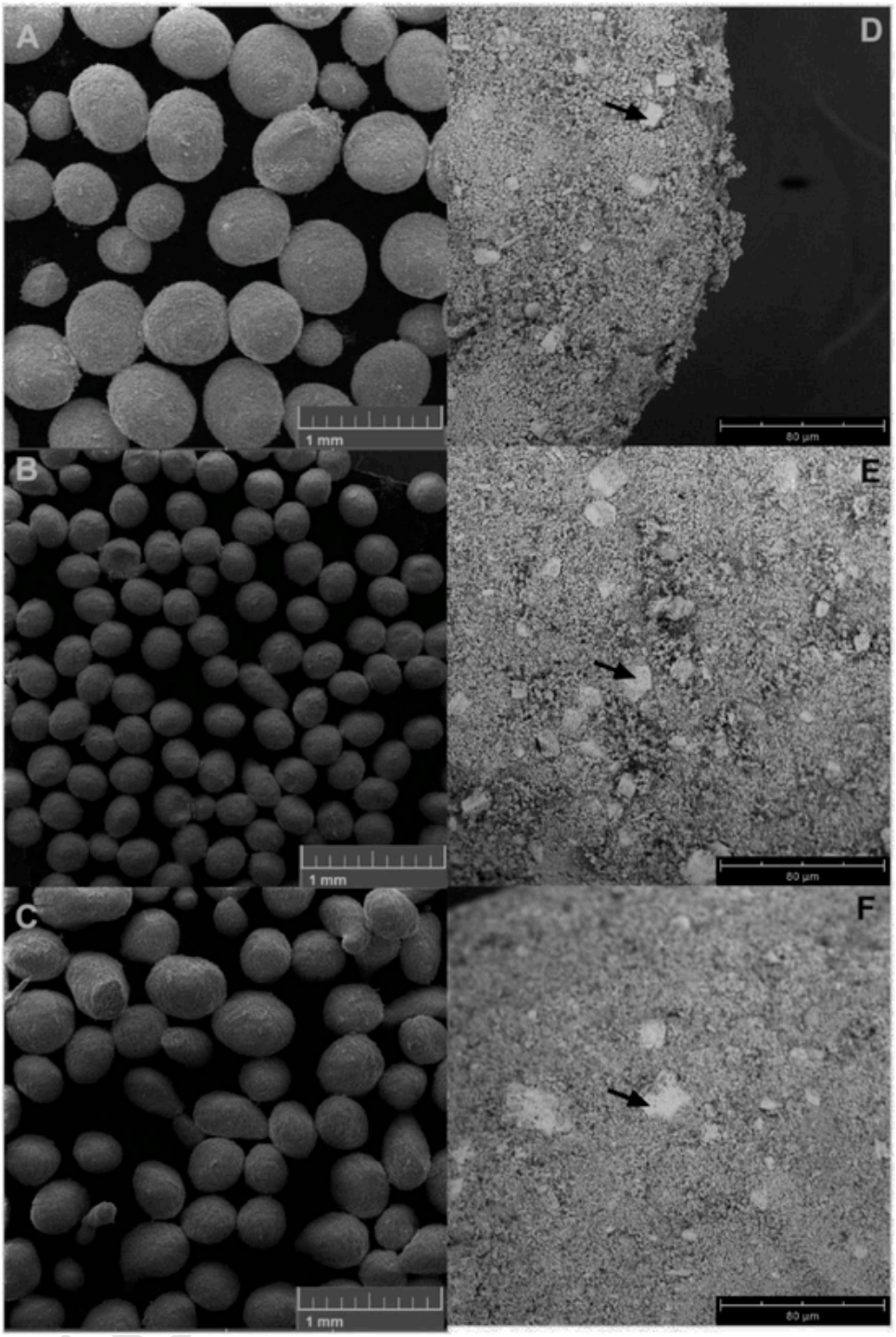

Fig. 4. SEM micrographs of the microspheres for measurements, A – 50 mL/h, B-70 mL/, C-90 mL/h, and from the solid phase surface obtained at flow rates of D – 50 mL/h, E- 70 mL/h and F - 90 mL/h.

3.3. Cytotoxicity of the studied IBS

The continuous phase had already been assessed by two preliminary tests, the MTT and Sulphordamine B assay. Considering previous results, on the first test, the continuous phase presented a cell viability above 70 % for RAW 267.4 cell line. The SRB test was performed on RAW 267.4 cell line and revealed no alterations on cell viability (Lima et al., 2018). Specifically, IBS cytotoxicity against L929 fibroblast was evaluated with sample that had the best result from injectability test. The results exhibit a cell viability of 95 ± 14 %, and, according to the BS EN ISO 10993-5: 2009 assay used, the IBS has a value above 70 % and is considered to be non-cytotoxic for this fibroblast cell line. According to other studies, inclusion of calcium phosphate elements did not produce cytotoxic results (Luo et al., 2020). Inclusion of bioglass on thermogelling chitosan hydrogel also did not produce cytotoxic response (Moreira et al., 2016).

Table 1
Summary of the rheological, mechanical and injectability properties of the four IBS formulations. Results with the same letter in the same line are not statistically different according to one-way ANOVA for 5% probability.

Rheological Properties					
	units	S1C1 (90 mL/h)	S1C1 (70 mL/h)	S1C0.8 (90 mL/h)	S1C08 (70 mL/h)
Consistency index	(Pa.s ^{n})	534	735	1900	2449
Flow behaviour index		0.55	0.68	0.71	0.8
R^2		99.87	99.76	99.98	99.76
Mechanical Properties					
Hardness	(N)	87 ± 3.92 ^{b}	90.98 ± 6.92 ^{b}	101 ± 5.21 ^{a}	103 ± 3.01 ^{a}
Cohesiveness	(N)	138 ± 1.32 ^{a}	141 ± 1.45 ^{a}	120 ± 1.04 ^{c}	124 ± 1.90 ^{b}
Compressibility	(N.mm)	46 ± 1.61 ^{b}	49 ± 3.06 ^{b}	56 ± 2.34 ^{a}	58 ± 2.76 ^{a}
Adhesiveness	(N.mm)	38 ± 2.02 ^{a}	39 ± 1.34 ^{a}	32 ± 1.43 ^{b}	33 ± 1.84 ^{b}
Injectability Properties					
Experimental Max Force	(N)	5.50	11.56	30.97	15.79
Theoretical Max Force	(N)	5.62	12.30	32.01	15.20

3.4. In vivo analysis

3.4.1. Postoperative observation

Throughout the evaluation period, the animals walked normally and did not show any degree of lameness, as well as little sensitivity to the operated area by touch, related to the smaller size of the bone lesion, the employed analgesia and minimal trauma to adjacent tissues. At the time of suture removal (10 days postoperatively) a slight increase in volume of a granuloma measuring on average 0.8 cm was observed on top of the implant region in three of the nine animals', which is characteristic of a granulomatous inflammation possibly due to inert particles that are notorious initiators of granulomatous lesions. Histological analysis of these lesions revealed multifocal areas of necrosis surrounded by inflammatory infiltrate of heterophiles and macrophages (Fig. 5A–B).

Since no gelation was induced with this material it is possible that some infiltration of this solution overextended the damaged region such as the surface. Another attributed factor may be allied to chitosan activity which can activate macrophages (Gorzelanny, Pöppelmann, Pappelbaum, Moerschbacher, & Schneider, 2010), since it is part of IBS composition. Contamination of the product during its handling was ruled out, because it was found through cell culture the absence of microorganisms in the areas of inflammation. Surgical trauma alone causes tissue damage, which alters the local chemical composition with a decrease in pH and activation of cells such as active macrophages and neutrophils (Percival, McCarty, Hunt, & Woods, 2014), combined with the acidic pH of IBS and may have altered the biological response.

It was also possible to notice a greater inflammatory reaction in the control group (with the collagen membrane in between the implant and bone) which can be attributed to the enzymatic degradation by collagenase and digestion of these denaturation products that promotes chemotaxis for fibroblast migration to the inflammatory site (Postlethwaite, Seyer, & Kang, 1978).

3.4.2. Radiographs of the bone defects after implantation with IBS

Radiographs permitted to evaluate the bone regeneration from tibial defects; bone remodelling mean diameter from groups 30 and 60 days exhibited similar values ($p > 0.05$), only when comparing the means at 30 and 60 days to their radiographic controls a significant difference can be observed (Table 2 e Fig. 6) and this can be attributed to the action of BCP, which is an excellent osteoconductor thus favouring the process of earlier bone healing (Stastny et al., 2019).

At 60 days of bone growth assessment, although not statistically significant compared to 30 days group, the process of bone remodelling of neoformed tissue and substitution by mature bone justified the higher radiopacity found at this time period (Oryan, Alidadi, Bigham-Sadegh, & Meimandi-Parizi, 2017). From both groups at 30 and 60 days, the latter more intense, a radiopaque line defined at the defect site was visible within the radiograph images, indicating osteointegration.

3.4.3. Histological evaluation

Histology slides revealed a significant amount of the remaining biomaterial in the two groups and periods evaluated, but more evidently at 30 days (Fig. 5C and D) with no difference in relation to neoformed bone tissue between the groups only for the periods studied. At 30 days, there was a slight neovascularization and bone loss continuity at the implant region with irregular and thin bone trabeculae formation, marginalized by osteoblasts and reactive osteocytes as well as immature bone tissue emerging from the edges of the defect. There was a considerable amount of biomaterial in the defect region related to the IBS (Fig. 5C). In addition, a significant amount of the biomaterial was reabsorbed by osteoclasts, (Yuan, Li, de Bruijn, de Groot, & Zhang, 2000) inducing osteoconductivity, where osteoclasts reabsorb the material by phagocytosis and osteoblasts produces bone neoformation.

At 60 days, similar findings were observed, but in a greater intensity. The defects were filled with more compact bone trabeculae and immature bone tissue in greater quantity. It can be perceived mature bone tissue near the medullary region and trabecular bone towards the periosteal region (Fig. 5E and F), besides the presence of IBS that was also in the process of resorption; therefore, exhibiting a slow resorption which is expected from BCP with a low HAp/ β-TCP ratio that directly influences the reabsorption of this material (Salamanca et al., 2017).

Nonetheless, at both 30 and 60 days postoperatively, some points of contact from the biomaterial with the newly formed bone tissue was observed, without interposition of fibrous tissue which demonstrates a good osteointegration by the usage of bioceramics.

Findings obtained by optical microscope confirms the results obtained from SEM, which exhibited reminiscent biomaterial with bone neoformation, presence of newly formed bone tissue and degraded biomaterial granules (Fig. 7).

Fig. 7A shows changes in the surface of the microspheres solid phase, resulting from the biomineralization owned by osteoblastic cells, exhibiting signs of a good osseointegration (Wang, Wang et al., 2019). Fig. 7B exhibit osteoblastic cells that were performing biomineralization and bone tissue deposition beneath the surface of the biomaterial. In the images obtained from the samples submitted to polishing process (Fig. 8), the microspheres integrated with the host tissue, but show signs of an irregular surface due to its degradation and

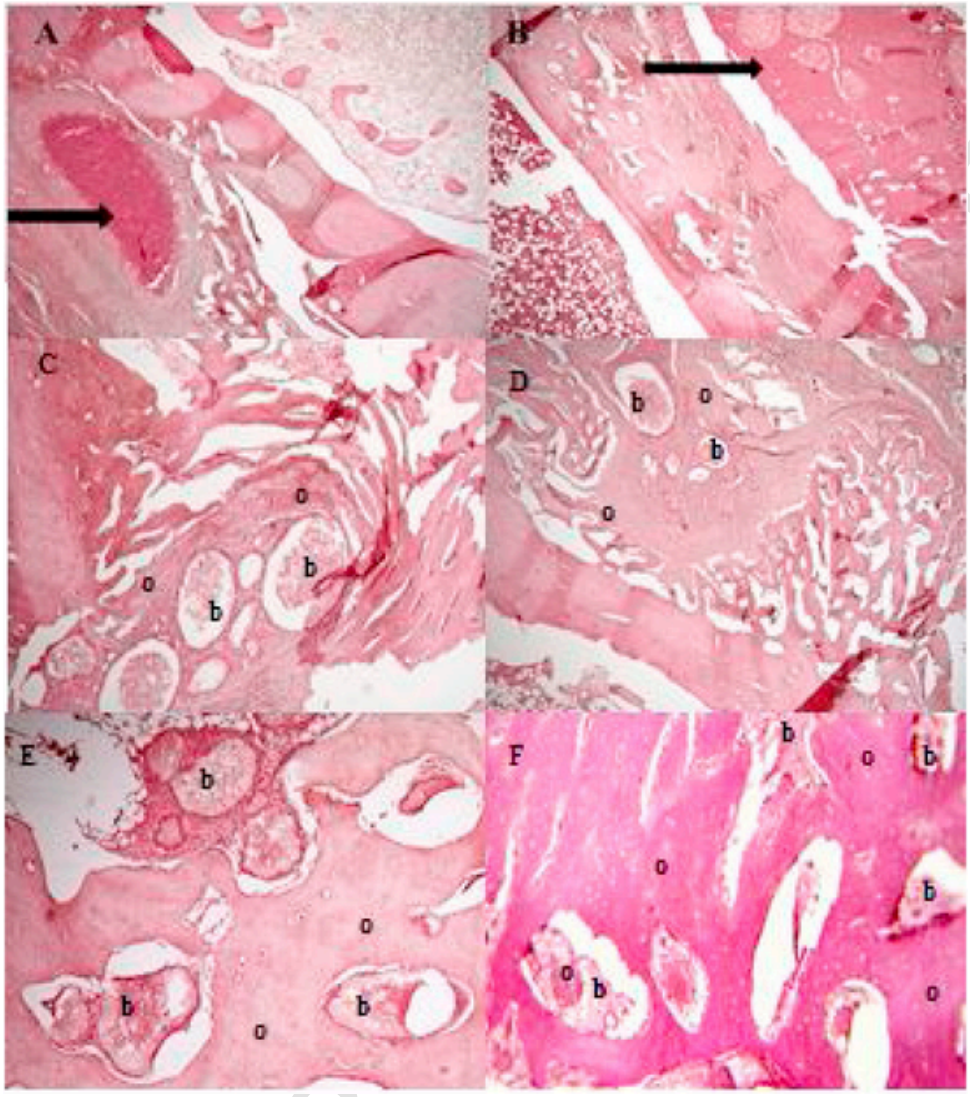

Fig. 5. Optical microscopy photograph of rabbit tibias (10 X), A - IBS-C group at 60 days and B - IBS group at 30 days postoperatively, the arrow shows inflammatory infiltrate around the implant granules with an area of necrosis. Figure C- IBS-C group at 30 days, D- IBS-C group at 60 days, E- IBS group at 30 days, F- IBS group at 60 days (b = biomaterial o = newly formed bone).

Table 2
Mean and standard deviation of bone thickness growth in mm measured by radiographic images.

Samples	30 days group			60 days group		
	Immediately after surgery	After 30 days	*p value*	Immediately after surgery	After 60 days	*p value*
IBS	0.47 ± 0.23	0.64 ± 0.17*	0.0033	0.44 ± 0.12	0.59 ± 0.15*	0.0051
IBS-C	0.52 ± 0.24	0.68 ± 0.20*	0.0033	0.37 ± 0.16	0.65 ± 0.15*	0.0022

* Statistically significant different from control.

leads to the appearance of IBS particles in the midst of bone neoformation. Presence of newly formed bones are observed and also interacts with the biomaterial, similar findings have been reported by the usage of BCP (Zhang et al., 2019).

No significant differences were observed in bone neoformation by the SEM technique between the time periods at 30 and 60 days with the IBS. One of the causes can be attributed to the size of the microspheres, as well as its density with low porosity used in this study. Smaller microspheres with larger interconnected pores may contribute to a greater bone resorption and neoformation over 30 and 60 days.

At 60 days post-surgery, biomaterials have not been fully reabsorbed, however, there are reports of remnants of bioceramics, HAp and β-TCP in bone defects in rabbit tibia 180 days after the operation ((Dalmônico et al., 2017)Dalmonico et al., 2017).

4. Conclusion

The work described herein proposes the usage of a material consisting of a solid phase - microspheres of biphasic calcium phosphate - and a liquid phase - polymeric solution of chitosan and polyethylene; the mixture of these two gives a pasty-like consistency material that can

Fig. 6. Radiographs of rabbit's tibias in craniocaudal projection, indicated by the circles are the sites of osteotomies. A, B, C and D - experimental groups with 30 days postoperatively. E, F, G and H - experimental groups at 60 days postoperatively. In figure A, B, E and F = Group IBS-C, in figure C, D, G and H = Group IBS. Figures A, C, E and G = immediate postoperative.

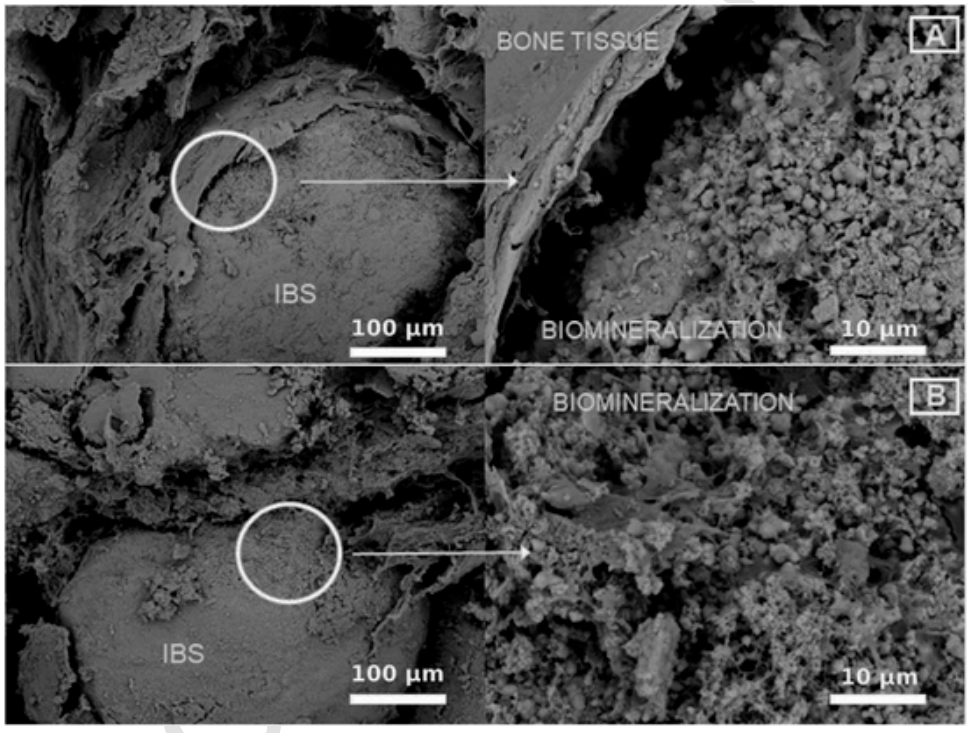

Fig. 7. SEM micrographs of the interface between the IBS and bone tissue. In A IBS group sample at 30 days and at B IBS samples, at 60 days postoperatively. It can be observed the presence of neoformed tissue and granules of the biomaterial in the process of degradation.

be injected using a syringe. By selective approaching these materials, it is possible to obtain a condition that is easily ejected from a syringe and that can not only be reabsorbed, but also have a good osteointegration in rabbit tibia bone defects. Although full regeneration and total re-absorption of the biomaterial was not verified at the time period of the study (60 days); this study correlates the fact that is possible to use a polymeric solution imbibed with microspheres for bone regeneration applications.

CRediT authorship contribution statement

Daniel Bezerra Lima: Conceptualization, Methodology, Visualization, Investigation. **Mônica Adriana Araújo de Souza:** Visualization, Investigation. **Gabriel Goetten de Lima:** Data curation, Writing - original draft, Visualization, Investigation. **Erick Platiní Ferreira Souto:** Visualization, Investigation. **Hugo Miguel Lisboa Oliveira:** Writing - review & editing. **Marcus Vinícius Lia Fook:** Conceptualization, Methodology. **Marcelo Jorge Cavalcanti de Sá:** Conceptualization, Methodology, Supervision.

Acknowledgement

This study was financed in part by the Coordenação de Aperfeiçoamento de Pessoal de Nível Superior - Brasil (CAPES) - Finance Code 001.

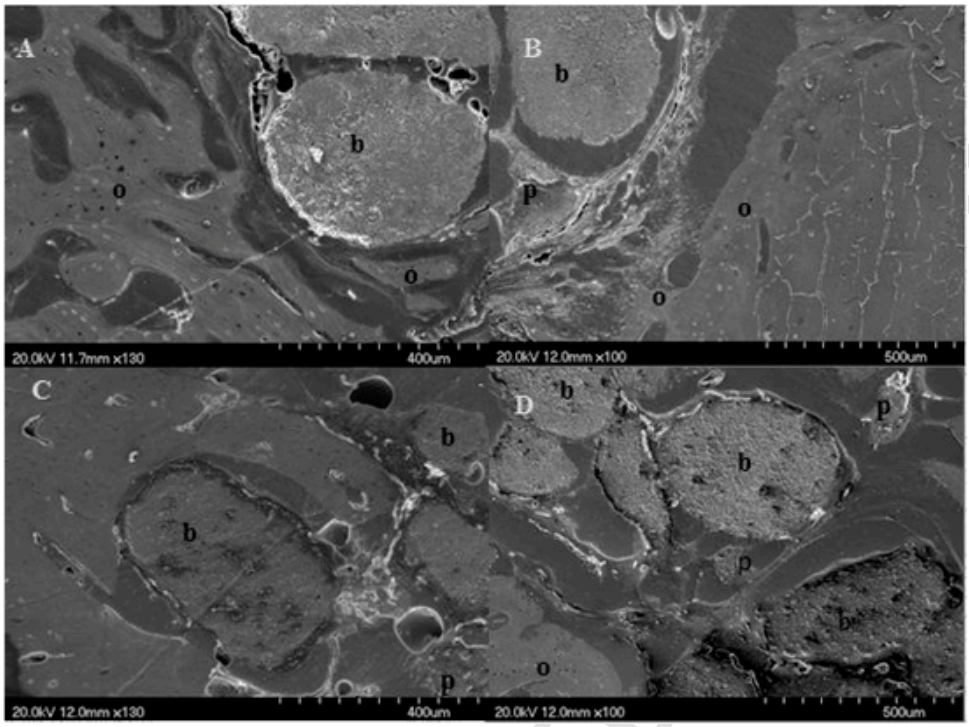

Fig. 8. SEM micrographs of polished samples sectioned at the implant interface. IBS-C group at 30 and 60 days (A and B) and IBS group at 30 and 60 days (C and D) in the postoperative period. (B = biomaterial, p = degraded biomaterial particles and o = bone neoformation).

References

Abueva, C D G, Jang, D-W, Padalhin, A, & Lee, B-T (2017). Phosphonate-chitosan functionalization of a multi-channel hydroxyapatite scaffold for interfacial implant-bone tissue integration. Journal of Materials Chemistry B, 5(6), 1293–1301. doi:10.1039/C6TB03228A.

Barbosa, W T, Almeida, K V, Lima, G G, Rodriguez, M A, Lia Fook, M V, García-Carrodeguas, R, … Sá, M J C (2020). Synthesis and in vivo evaluation of a scaffold containing wollastonite/β-TCP for bone repair in a rabbit tibial defect model. Journal of Biomedical Materials Research Part B: Applied Biomaterials, 108(3), 1107–1116. doi:10.1002/jbm.b.34462.

Batista, H A, Silva, F N, Lisboa, H M, & Costa, A C F M (2020). Modeling and optimization of combustion synthesis for hydroxyapatite production. Ceramics International, 46(8), 11638–11646. doi:10.1016/j.ceramint.2020.01.194.

Bencherif, S A, Sands, R W, Bhatta, D, Arany, P, Verbeke, C S, Edwards, D A, … Mooney, D J (2012). Injectable preformed scaffolds with shape-memory properties. Proceedings of the National Academy of Sciences, 109(48), 19590–19595. doi:10.1073/pnas.1211516109.

Bezerril, L M, de Vasconcelos, C L, Dantas, T N C, Pereira, M R, & Fonseca, J L C (2006). Rheology of chitosan-kaolin dispersions. Colloids and Surfaces A: Physicochemical and Engineering Aspects, 287(1–3), 24–28. doi:10.1016/j.colsurfa.2006.03.017.

Canillas, M, Pena, P, de Aza, A H, & Rodríguez, M A (2017). Calcium phosphates for biomedical applications. Boletín de La Sociedad Española de Cerámica y Vidrio, 56(3), 91–112. doi:10.1016/j.bsecv.2017.05.001.

Cordova, L A, Stresing, V, Gobin, B, Rosset, P, Passuti, N, Gouin, F, … Heymann, D (2014). Orthopaedic implant failure: Aseptic implant loosening–The contribution and future challenges of mouse models in translational research. Clinical Science, 127(5), 277–293. doi:10.1042/CS20130338.

Daculsi, G (1998). Biphasic calcium phosphate concept applied to artificial bone, implant coating and injectable bone substitute. Biomaterials, 19(16), 1473–1478.

Dalmônico, G M L, Franczak, P F, Levandowski , Camargo, N H A, Dallabrida, A L, da Costa, B D, … Canillas, M (2017). An in vivo study on bone formation behavior of microporous granular calcium phosphate, 5(7), 1315–1325. doi:10.1039/C7BM00162B.

Di Martino, A, Sittinger, M, & Risbud, M V (2005). Chitosan: A versatile biopolymer for orthopaedic tissue-engineering. Biomaterials, 26(30), 5983–5990. doi:10.1016/j.biomaterials.2005.03.016.

Drug, D P I D P I (1998). Guidance for industry. Center for Drug Evaluation and Research (CDER). 1000.

Gorzelanny, C, Pöppelmann, B, Pappelbaum, K, Moerschbacher, B M, & Schneider, S W (2010). Human macrophage activation triggered by chitotriosidase-mediated chitin and chitosan degradation. Biomaterials, 31(33), 8556–8563. doi:10.1016/j.biomaterials.2010.07.100.

Hasan, M L, Kim, B, Padalhin, A R, Faruq, O, Sultana, T, & Lee, B-T (2019). In vitro and in vivo evaluation of bioglass microspheres incorporated brushite cement for bone regeneration. Materials Science and Engineering: C, 103, 109775. doi:10.1016/j.msec.2019.109775.

Jahan, K, Mekhail, M, & Tabrizian, M (2019). One-step fabrication of apatite-chitosan scaffold as a potential injectable construct for bone tissue engineering. Carbohydrate Polymers, 203, 60–70. doi:10.1016/j.carbpol.2018.09.017.

Kokubo, T (2008). Bioceramics and their clinical applications. Elsevier.

Kraal, T, Mullender, M, de Bruine, J H D, Reinhard, R, de Gast, A, Kuik, D J, … van Royen, B J (2008). Resorbability of rigid beta-tricalcium phosphate wedges in open-wedge high tibial osteotomy: A retrospective radiological study. The Knee, 15(3), 201–205. doi:10.1016/j.knee.2008.02.005.

Lal, P, & Sun, W (2004). Computer modeling approach for microsphere-packed bone scaffold. Computer-Aided Design, 36(5), 487–497. doi:10.1016/S0010-4485(03)00134-9.

Lee, D W, Lim, C, Israelachvili, J N, & Hwang, D S (2013). Strong adhesion and cohesion of chitosan in aqueous solutions. Langmuir, 29(46), 14222–14229. doi:10.1021/la403124u.

Lee, G H, Makkar, P, Paul, K, & Lee, B (2017). Incorporation of BMP-2 loaded collagen conjugated BCP granules in calcium phosphate cement based injectable bone substitutes for improved bone regeneration. Materials Science and Engineering: C, 77, 713–724. doi:10.1016/j.msec.2017.03.296.

Legeros, R Z, Lin, S, Rohanizadeh, R, Mijares, D, & Legeros, J P (2003). Biphasic calcium phosphate bioceramics: Preparation, properties and applications. Journal of Materials Science: Materials in Medicine. doi:10.1023/A:1022872421333.

Li, Y, Zhang, Z, & Zhang, Z (2018). Porous chitosan/nano-hydroxyapatite composite scaffolds incorporating simvastatin-loaded PLGA microspheres for bone repair. Cells, Tissues, Organs, 205(1), 20–31. doi:10.1159/000485502.

Lima, D B, Almeida, R D, Pasquali, M, Borges, S P, Fook, M L, & Lisboa, H M (2018). Physical characterization and modeling of chitosan/peg blends for injectable scaffolds. Carbohydrate Polymers, 189, 238–249. doi:10.1016/j.carbpol.2018.02.045.

Luo, C, Wu, S, Li, J, Li, X, Yang, P, & Li, G (2020). Chitosan/calcium phosphate flower-like microparticles as carriers for drug delivery platform. International Journal of Biological Macromolecules, 155, 174–183. doi:10.1016/j.ijbiomac.2020.03.172.

Matinfar, M, Mesgar, A S, & Mohammadi, Z (2019). Evaluation of physicochemical, mechanical and biological properties of chitosan/carboxymethyl cellulose reinforced with multiphasic calcium phosphate whisker-like fibers for bone tissue engineering. Materials Science and Engineering: C, 100, 341–353. doi:10.1016/j.msec.2019.03.015.

Mitschka, P (1982). Simple conversion of Brookfield R.V.T. readings into viscosity functions. Rheologica Acta, 21(2), 207–209. doi:10.1007/BF01736420.

Moreira, C D F, Carvalho, S M, Mansur, H S, & Pereira, M M (2016). Thermogelling chitosan–collagen–bioactive glass nanoparticle hybrids as potential injectable systems for tissue engineering. Materials Science and Engineering: C, 58, 1207–1216. doi:10.1016/j.msec.2015.09.075.

Nam, S-B, Bae, Y-C, Moon, J-S, & Kang, Y-S (2006). Analysis of the postoperative outcome in 405 cases of orbital fracture using 2 synthetic orbital implants. Annals of Plastic Surgery, 56(3), 263–267.

Oryan, A, Alidadi, S, Bigham-Sadegh, A, & Meimandi-Parizi, A (2017). Chitosan/gelatin/platelet gel enriched by a combination of hydroxyapatite and beta-tricalcium phosphate in healing of a radial bone defect model in rat. International Journal of Biological Macromolecules, 101, 630–637. doi:10.1016/j.ijbiomac.2017.03.148.

Percival, S L, McCarty, S, Hunt, J A, & Woods, E J (2014). The effects of pH on wound healing, biofilms, and antimicrobial efficacy. Wound Repair and Regeneration, 22(2), 174–186.

Pon-On, W, Suntornsaratoon, P, Charoenphandhu, N, Thongbunchoo, J, Krishnamra, N, & Tang, I M (2016). Hydroxyapatite from fish scale for potential use as bone scaffold or regenerative material. Materials Science and Engineering: C, 62, 183–189. doi:10.1016/j.msec.2016.01.051.

Postlethwaite, A E, Seyer, J M, & Kang, A H (1978). Chemotactic attraction of human fibroblasts to type I, II, and III collagens and collagen-derived peptides. Proceedings of the National Academy of Sciences, 75(2), 871–875. doi:10.1073/pnas.75.2.871.

R Core Team (2015). R: A Language and Environment for Statistical Computing. Vienna, Austria: R Foundation for Statistical Computing.

Ramirez Caballero, S S, Saiz, E, Montembault, A, Tadier, S, Maire, E, David, L, … Grémillard, L (2019). 3-D printing of chitosan-calcium phosphate inks: Rheology, interactions and characterization. Journal of Materials Science: Materials in Medicine, 30(1), 6. doi:10.1007/s10856-018-6201-y.

Rangavittal, N, Landa-Canovas, A R, Gonzalez-Calbet, J M, & Vallet-Regí, M (2000). Structural study and stability of hydroxyapatite and β-tricalcium phosphate: Two important bioceramics. Journal of Biomedical Materials Research, 51(4), 660–668.

Salamanca, E, Pan, Y-H, Tsai, A, Lin, P-Y, Lin, C-K, Huang, H-M, … Chang, W-J (2017). Enhancement of osteoblastic-like cell activity by glow discharge plasma surface modified hydroxyapatite/β-tricalcium phosphate bone substitute. Materials, 10(12), 1347. doi:10.3390/ma10121347.

Saravanan, S, Vimalraj, S, Thanikaivelan, P, Banudevi, S, & Manivasagam, G (2019). A review on injectable chitosan/beta glycerophosphate hydrogels for bone tissue regeneration. International Journal of Biological Macromolecules, 121, 38–54. doi:10.1016/j.ijbiomac.2018.10.014.

Stastny, P, Sedlacek, R, Suchy, T, Lukasova, V, Rampichova, M, & Trunec, M (2019). Structure degradation and strength changes of sintered calcium phosphate bone scaffolds with different phase structures during simulated biodegradation in vitro. Materials Science and Engineering: C, 100, 544–553. doi:10.1016/j.msec.2019.03.027.

Taz, M, Makkar, P, Imran, K M, Jang, D W, Kim, Y-S, & Lee, B-T (2019). Bone regeneration of multichannel biphasic calcium phosphate granules supplemented with hyaluronic acid. Materials Science and Engineering: C, 99, 1058–1066. doi:10.1016/j.msec.2019.02.051.

Thai, V V, & Lee, B-T (2010). Fabrication of calcium phosphate–calcium sulfate injectable bone substitute using hydroxy-propyl-methyl-cellulose and citric acid. Journal of Materials Science: Materials in Medicine, 21(6), 1867–1874. doi:10.1007/s10856-010-4058-9.

Thangavelu, M, Adithan, A, John Peter, J S, Hossain, M A, Kim, N S, Hwang, K-C, … Kim, J-H (2019). Ginseng compound K incorporated porous Chitosan/biphasic calcium phosphate composite microsphere for bone regeneration. International Journal of Biological Macromolecules. doi:10.1016/j.ijbiomac.2019.09.228.

Wang, Y, Pan, J, Zhang, Y, Li, X, Zhang, Z, Wang, P, … Li, J (2019). Wnt and Notch signaling pathways in calcium phosphate-enhanced osteogenic differentiation: A pilot study. Journal of Biomedical Materials Research Part B: Applied Biomaterials, 107(1), 149–160. doi:10.1002/jbm.b.34105.

Wang, J, Wang, M, Chen, F, Wei, Y, Chen, X, Zhou, Y, … Zhang, X (2019). Nano-hydroxyapatite coating promotes porous calcium phosphate ceramic-induced osteogenesis via BMP/Smad signaling pathway. International Journal of Nanomedicine, 14, 7987–8000. doi:10.2147/IJN.S216182.

Yuan, H, Li, Y, de Bruijn, J, de Groot, K, & Zhang, X (2000). Tissue responses of calcium phosphate cement: A study in dogs. Biomaterials, 21(12), 1283–1290. doi:10.1016/S0142-9612(00)00016-8.

Zhang, Z, Wang, P, Li, X, Wang, Y, Qin, Z, Zhang, C, … Li, J (2019). Reconstruction of mandibular bone defects using biphasic calcium phosphate bone substitutes with simultaneous implant placement in mini-swine: A pilot in vivo study. Journal of Biomedical Materials Research Part B: Applied Biomaterials, 107(6), 2071–2079. doi:10.1002/jbm.b.34299.